Bulletin of the Seismological Society of America, Vol. 99, No. 2A, pp. 647–663, April 2009, doi: 10.1785/0120080240

Uncertainties in Strong Ground-Motion Prediction with Finite-Fault Synthetic Seismograms: An Application to the 1984 *M* 5.7 Gubbio, Central Italy, Earthquake

by Gabriele Ameri, František Gallovič, Francesca Pacor, and Antonio Emolo

Abstract This study investigates the engineering applicability of two conceptually different finite-fault simulation techniques. We focus our attention on two important aspects: first to quantify the capability of the methods to reproduce the observed ground-motion parameters (peaks and integral quantities); second to quantify the dependence of the strong-motion parameters on the variability in the large-scale kinematic definition of the source (i.e., position of the nucleation point, value of the rupture velocity, and distribution of the final slip on the fault).

We applied an approximated simulation technique, the deterministic-stochastic method and a broadband technique, the hybrid-integral-composite method, to model the 1984 M_w 5.7 Gubbio, central Italy, earthquake, at five accelerometric stations. We first optimize the position of the nucleation point and the value of the rupture velocity for three different final slip distributions on the fault by minimizing an error function in terms of acceleration response spectra in the frequency band from 1 to 9 Hz. We found that the best model is given by a rupture propagating at about 2.65 km/sec from a hypocenter located approximately at the center of the fault. In the second part of the article we calculate more than 2400 scenarios varying the kinematic source parameters. At the five sites we compute the residuals distributions for the various strong-motion parameters and show that their standard deviations depend on the source parameterization adopted by the two techniques. Furthermore, we show that Arias Intensity (AI) and significant duration are characterized by the largest and smallest standard deviation, respectively. Housner Intensity is better modeled and less affected by uncertainties in the source kinematic parameters than AI. The fact that the uncertainties in the kinematic model affects the variability of different ground-motion parameters in different ways has to be taken into account when performing hazard assessment and earthquake engineering studies for future events.

Introduction

Earthquake engineering analysis requires, as seismic input, a reliable and complete characterization of ground motion both in time and frequency domains. This information is needed especially with the increasing number of applications of nonlinear analysis techniques aimed at assessing the structural response and damage estimation from future seismic events. For time-series analysis, engineers often use a suite of natural accelerograms from past earthquakes that, based on certain selection criteria (magnitude, distance, site class, strong-motion parameter, tectonic environment, spectral matching, etc.), are suitable for the purpose (Stewart *et al.*, 2001; Bommer and Acevedo, 2004; Iervolino and Cornell, 2005). For other applications, such as hazard assessment or linear analysis for loss estimations in urban areas, the whole time series is not always necessary and an instantaneous measure of motion (e.g., peak ground acceleration [PGA]) could represent a satisfactory description. The level of ground motion for a particular site is generally assessed by means of ground motion prediction equations, where a ground-motion parameter (in general PGA, peak ground velocity [PGV], or spectral acceleration) is provided as a function of magnitude, distance, and site condition (Douglas, 2003 and references therein). In both cases the prediction of ground motion from future events can, thus, be estimated by using data recorded during past earthquakes.

It is accepted today that problems arise from the use of recorded data for prediction of future ground motions. Indeed, despite the huge growth of the recorded database dur-

ing the last years due to the increasing number of strong-motion networks installed in high-seismicity areas, the set of existing recordings always represents only a subset of possible earthquake scenarios. Consequently, the greater the number of parameters to be specified for the selection of natural accelerograms, the lower the number of them that will be extracted from the strong-motion database for the specific analysis. To keep this number reasonable (i.e., statistically significant), engineers are compelled to either reduce the number of searching criteria or expand the limits of the searching window (e.g., in terms of magnitude and distance). Moreover, the records should generally be scaled and/or modified to match (with some specified level of agreement) the elastic design spectrum prescribed by the adopted seismic code. This manipulation is, however, a thorny problem. For example, in case that the structure is located on a particular soil condition (e.g., basin), adjusting or scaling the spectral amplitude of a signal recorded on a rock site would never provide information on the long duration actually generated.

Several studies (e.g., Archuleta and Hartzell, 1981; Somerville *et al.*, 1997; Shakal *et al.*, 2006) have shown that, at distances comparable with few fault lengths and at frequencies of engineering interest, the finite-fault effects (directivity effects, fling step, hanging-wall/footwall effects, low-frequency pulses, radiation-pattern effects, etc.) are not negligible. The near-source ground motion from moderate-to-large events is strongly affected by the evolution of the rupture along the extended fault, causing complex spatial distribution of the observed values. The ground-motion variability close to the seismic source cannot be reproduced by empirical models accounting only for average characteristics of the motion.

An alternative to the use of records from past earthquakes comes from the advances in understanding the earthquake source and wave propagation processes. Numerical techniques, based on a kinematic source description, can be used to simulate realistic synthetic seismograms for engineering needs (Graves and Pitarka, 2004; Pacor *et al.*, 2005; Liu *et al.*, 2006; Gallovič and Brokešová, 2007; Ameri *et al.*, 2008; among many others). One advantage of such techniques is that once the amplification due to local geology is taken into account, the synthetic time series can be directly used; they result from a given earthquake scenario with selected magnitude, distance, propagation model, site conditions, and so on and do not need to be scaled or modified for any further applications.

However, these models require the definition of a large number of input physical parameters whose values rarely can be fixed *a priori*, leading to a limit on their use for studies related to prediction of ground motion. Indeed, even if we are usually able to identify a causative fault and to retrieve information on the propagation medium, we are not able to determine, for example, the rupture velocity, the space-time distribution of slip over the fault plane, or the position of the rupture starting point. To handle this principle lack of knowledge we are compelled either to make a strong assumption on the value of each kinematic parameter or to generate a large number of shaking scenarios (all equally probable) trying to constrain the input values to plausible ranges. While in the first case we generate a single earthquake scenario that is, anyway, only one of the possible realization without any statistical significance, in the latter we generate a number of ground-motion parameters for each site that, although complicated to manage for specific engineering purposes, can be statistically analyzed to infer some insights on the probability distributions of ground-motion values and related statistical estimators (mean, median, mode, standard deviation, etc.).

In this article we investigate the engineering applicability of two conceptually different kinematic simulation techniques. We focus our attention on two issues: first to quantify the capability of each method to reproduce the earthquake ground-motion parameters usually required for engineering analysis (e.g., PGA, PGV, spectral acceleration, Arias Intensity [AI], Housner Intensity [HI], and significant duration [T90]); second to quantify how the predicted values depend on the variability in the large-scale kinematic description of the source (i.e., position of the nucleation point, value of the rupture velocity, and distribution of the final slip on the fault).

The sensitivity of ground motion to the source parameters has been studied by several authors (Pavic *et al.*, 2000; Gallovič and Brokešová, 2004; Hartzell *et al.*, 2005; Sørensen *et al.*, 2007; Ripperger *et al.*, 2008; Wang *et al.*, 2008). However, only few studies evaluate how the uncertainties in the source parameterization propagates to ground-motion estimates also using different modeling approaches, and even fewer attempt to assess how the different ground-motion parameters are affected by these uncertainties.

The selected case study is the 1984 (M_w 5.7) Gubbio earthquake (central Italy), for which five near-source strong-motion records are available. This earthquake represents a typical moderate magnitude event, occurring in central Italy, where the scarcity of records and the important role of site amplification at the recording stations make the studies related to the earthquake rupture process and to ground-motion modeling particularly complicated. The analyses have been performed within the project titled S3—Shaking and damage scenarios in area of strategic and/or priority interest, developed in the frame of the 2004–2006 agreement between the Istituto Nazionale di Geofisica e Vulcanologia (INGV, National Institute of Geophysics and Volcanology) and the Dipartimento della Protezione Civile (Italian Department of Civil Protection) where the modeling of the reference earthquakes was aimed at computing shaking scenarios for the Gubbio town and the nearby basin (S3 Project, 2007, Deliverable D20).

Here, we present the modeling of the 1984 Gubbio earthquake at the five accelerometric stations, applying two different finite-fault simulation methods, namely the deterministic-stochastic method (DSM, Pacor *et al.*, 2005) and the hybrid-integral-composite method (HIC, Gallovič and Brokešová, 2007). We first optimize the model source

parameters in order to infer the best scenario fitting the observed data and to evaluate the capability of each technique to reproduce strong-motion parameters of engineering interest (peaks and integral values). In the second part of the article we analyze the strong-motion parameters distributions retrieved at each site from the computation of more than 2400 scenarios varying the source kinematic parameters. The obtained variability is then discussed both in terms of the simulation techniques and of the specific strong-motion parameter.

Source Model, Strong-Motion Data, and Site Effects

The Gubbio area (northern Umbria region, central Italy) is characterized by moderate magnitude earthquakes. The 29 April 1984 (5:03 UTC) earthquake struck the Gubbio and surrounding municipalities with moment magnitude M_w 5.7 and, to date, it is the strongest event recorded in the area.

The source of this event is related to the rupture of a segment of the Gubbio fault, considered to be an active fault (Mirabella *et al.*, 2004). The Gubbio fault is part of the seismogenic Umbrian fault system, which consists of a set of aligned north-northwest–south-southeast trending, southwest dipping normal faults. Based on the integration of geologic, geomorphic, and seismological data, Pucci *et al.* (2003) suggested that the low-angle Gubbio fault is formed by two individual segments capable of generating M 5.3–5.9 earthquakes (Fig. 1). The southern segment ruptured during the 1984 earthquake while the northern segment did not rupture recently nor historically. These two segments are also cataloged in the Database of Individual Seismogenic Sources (DISS v. 3.0.4) for Italy and some surrounding countries (see the Data and Resources section).

The source model adopted in this study corresponds to the rupture of the southern segment of the Gubbio fault (identified as ITGG037 in the DISS v. 3.0.4 database); however, we use a modified fault (hereinafter ITGG037mod) because in 1984 the earthquake apparently did not rupture the whole ITGG037 fault. The source dimensions were assigned following the scaling relations of Wells and Coppersmith (1994) while the seismic moment was calculated basing on the Hanks and Kanamori (1979) relations. The source characteristics of the ITGG037 and ITGG037mod faults are listed in Table 1.

The 1D propagation model for the Gubbio area (Table 2) has been extracted from a 3D-tomography study based on the inversion of P and S minus P arrival times from seismic records of the INGV network (M. Moretti and P. De Gori, personal comm., 2006; S3 Project 2007, Deliverable D20). The anelastic attenuation is implemented differently in each simulation method. We use a frequency-dependent Q_S function in DSM modeling and standard Q_P and Q_S values for each crustal layer in HIC modeling. Various studies on the attenuation properties are available for the area (Malagnini and Herrmann, 2000; Bindi *et al.*, 2004; Castro *et al.*, 2004). They are mainly based on the data set of seismic recordings collected during the 1997–1998 Umbria-Marche seismic sequence (M_{max} 6.0). We adopt the results from Castro *et al.* (2004)

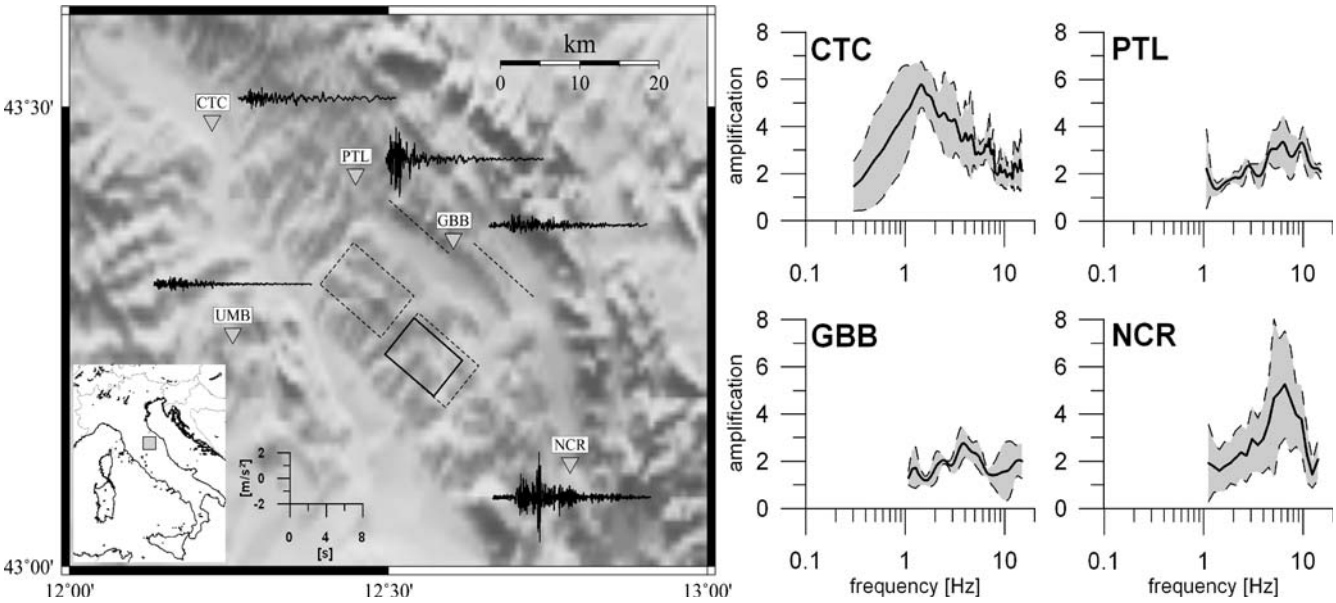

Figure 1. Accelerometric stations (gray triangles) triggered by the 1984 Gubbio earthquake and the Gubbio fault geometry; the dashed rectangles represent the surface projection of the fault plane. Dashed lines represent the hypothetical surface fault trace. The portion of the Gubbio fault used to simulate the 1984 earthquake is shown as a thick rectangle. For each station the north–south component of the recorded seismogram is presented. The four plots in the right-hand panel of the figure represent the HVSRs (mean ± 1standard deviation) determined for the accelerometric stations. The HVSRs computed at PTL, NCR, and GBB are considered reliable in the frequency range 1–15 Hz. Note that no HVSR is presented for the UMB station due to the lack of records.

Table 1
Fault Parameters Assumed for the 1984 Earthquake

Characteristics	ITGG037	ITGG037mod*
Length (km)	10.0	8.0
Width (km)	7.0	6.0
Strike (°)	130	130
Dip (°)	20	20
Rake (°)	−90	−90
Top depth (km)	4.0	4.3
Bottom depth (km)	6.4	6.4
Seismic moment (N m)	1.05×10^{18}	4.32×10^{17}
Moment magnitude	6.0	5.7
Mean slip (m)	0.5	0.3

See the Data and Resources section for information on the database for these events.

*Fault modified to fit the 1984 earthquake magnitude.

who performed a parametric inversion on the *S*-wave windows of the entire Umbria-Marche strong-motion data set that also includes accelerometric stations installed in the Gubbio area (i.e., GBB and GBP, located inside and nearby the basin). Castro *et al.* (2004) obtained a quality factor Q, representative of the *S*-wave train, approximated by the relation $Q_S = 31.2f^{1.2}$ up to $f = 9.0$ Hz. At higher frequencies the Q_S takes a nearly constant value of about 438 (see Table 2), which can adequately model the high-frequency attenuation near the site (κ parameter) as suggested by the authors themselves.

Five accelerometric stations belonging to the Italian strong motion network (RAN, Rete Accelerometrica Nazionale) were triggered by the 1984 Gubbio earthquake. Figure 1 shows a map of the study area together with the position of the stations and of the ITGG037mod fault. For each station, the north–south components of the recorded acceleration time series is also shown.

All stations were equipped with analog instruments. The data were corrected for the instrumental response and filtered with a cosine band-pass filter. The high-pass frequency was selected by visual inspection of the uncorrected Fourier spectrum. For all data it was set around 0.25 Hz, with the exception of the Umbertide (UMB) station waveforms that were filtered at 1 Hz because of high noise level. For the comparison with synthetic data, a low-pass filter at 10 Hz was applied, and time windows that start 1 sec before the first *S*-wave arrival and contain 85% of the energy of the records were used. These time windows were chosen with the aim of eliminating phases different from *S* waves as, for instance, the locally generated surface waves at the Città di Castello (CTC) station (see Fig. 1), which we are unable to model with the present crustal model. Strong-motion parameters computed from the processed data are reported in Table 3. The maximum acceleration (1.85 m/sec^2) was recorded at Nocera Umbra station (NCR), located about 20 km southeast from the fault, while the minimum one (0.20 m/sec^2) was observed at UMB, located about 25 km in the opposite direction. These differences in amplitudes can be ascribed in principle both to source and site effects.

Table 2
1D Propagation Model Adopted in Simulations*

Depth (km)	V_P (km/sec)	V_S (km/sec)	rho (kg/m^3)	Q_P	Q_S
0.00	4.05	2.17	2400	200	100
1.00	4.62	2.47	2400	200	100
2.00	5.19	2.76	2400	300	150
3.00	5.86	3.10	2750	600	300
5.00	6.20	3.33	2750	600	300
6.00	6.40	3.50	2750	600	300
12.00	6.50	3.53	2750	1000	500
24.00	6.60	3.59	2750	1000	500

The $Q_S(f)$ values from Castro *et al.* (2004) are used in the DSM simulations while frequency independent Q_P and Q_S values are used in the HIC simulations. $Q_S(f) = 31.2f^{1.2}$ for $f < 9.0$ Hz and $Q_S(f) = 438$ for $f > 9.0$ Hz.

*M. Moretti and P. De Gori, personal comm., 2006; S3 Project 2007, Deliverable D20

In the Umbria-Marche area, the site effects play an important role. Various authors (Bindi *et al.*, 2004; Castro *et al.*, 2004; Luzi *et al.*, 2005) exploited strong-motion data recorded mainly during the Umbria-Marche seismic sequence (1997–1998) to investigate site response in the area, providing both empirical and theoretical transfer functions for some of the accelerometric stations. Unfortunately, complete information on site amplification was not available for all the five stations used in this study. Detailed investigations are available for NCR (Marra *et al.*, 2000; Rovelli *et al.*, 2002; Cultrera *et al.*, 2003) and for GBB (Luzi *et al.*, 2005). Although both stations are located on shallow alluvial covers with $V_S < 360$ m/sec (Cattaneo and Marcellini, 2000; Luzi *et al.*, 2005), NCR is characterized by a very complex response site with strong amplification at frequencies higher than 5 Hz due to the presence of a buried wedge of weathered rock underlying the station (Rovelli *et al.*, 2002; Cultrera *et al.*, 2003).

In order to take into account site amplification at each site, we estimated average spectral ratios between horizontal and vertical components of ground motion (horizontal-vertical spectral ratio (HVSR) method; Lermo and Chávez-García, 1993; Field and Jacob, 1995) using the available accelerometric recordings from the database of the Italian strong-motion data (see the Data and Resources section; Fig. 1, right-hand panel). We are aware that the HVSRs do not provide the actual site transfer function but we decided to use them as the best information currently available to take into account site amplification at all stations used in this study. Furthermore, for NCR and GBB the fundamental frequencies and amplification factor detected with the HVSR method are in agreement with those estimated by other empirical techniques based on reference sites (i.e., generalized spectral inversion technique) as shown by Castro *et al.* (2004) and Luzi *et al.* (2005).

For NCR and GBB stations the HVSRs are well constrained (with five or more events recorded at the station) while at Pietralunga (PTL) the spectral ratio is computed

Table 3

Ground-Motion Parameters Computed for the *S*-Wave Time Window are Shown for Each Station and for Both Horizontal Components

Station Name	Horizontal Component	R_{hypo} (km)	PGA (m/sec^2)	PGV (m/sec)	AI (m/sec)	HI (m)	T90 (sec)
CTC	North–South	38.6	0.34	0.018	0.0080	0.056	3.2
	East–West		0.39	0.027	0.013	0.1	3
GBB	North–South	17.8	0.48	0.035	0.021	0.1	6.2
	East–West		0.72	0.034	0.035	0.12	4.9
NCR	North–South	21.5	1.8	0.048	0.12	0.076	3.5
	East–West		1.5	0.058	0.093	0.094	5.2
PTL	North–South	26.8	1.3	0.055	0.1	0.17	2.5
	East–West		1.4	0.080	0.11	0.2	3.3
UMB	North–South	26.5	0.21	0.0090	0.0040	0.023	3.8
	East–West		0.2	0.010	0.0040	0.023	4

Definitions of the column headings are as follows: hypocentral distance, R_{hypo}; peak ground acceleration, PGA; peak ground velocity, PGV; Arias Intensity, AI; Housner Intensity, HI; significant duration, T90. Waveforms are band-pass filtered as described in the text.

using only 3 recordings and has to be considered poorly constrained. For the UMB station the HVSR calculated with the only available record reports an amplification peak at about 15 Hz and lower amplifications (about a factor of 2) for frequencies below 10 Hz. Because only one record is used, the HVSR method cannot provide a statistically significant site amplification function and, therefore, we decided not to use it. In any case, this site is reported to be stiff soil or rock (Luzi *et al.*, 2005; Bindi *et al.*, 2006) and no large amplifications are expected. The CTC station is located on a very deep basin (Bordoni *et al.*, 2003), and it may not be appropriate to estimate the response site with the HVSRs as the vertical component of motion could be affected by amplification violating the fundamental assumption on which this technique is based (Castro *et al.*, 2004; Pacor *et al.*, 2007). In this case we used the empirical transfer function obtained by averaging standard spectral ratios for an array of stations located around the accelerometric station (Bordoni *et al.*, 2003; L. Luzi, personal comm., 2007).

As shown in the right-hand panel of Figure 1, the NCR station is strongly influenced by site effects with an amplification up to 8 (mean plus one standard deviation) at about 6 Hz. The CTC station is characterized by high-amplification values at low frequencies (around 1 Hz) related to the generation of low-frequency phases within the Città di Castello basin (Bordoni *et al.*, 2003). PTL and GBB sites are characterized by modest amplification values at 5–6 Hz.

Methods

The two kinematic modeling techniques applied in this study are briefly described in order to better understand the results presented in the article and to highlight differences in their modeling philosophy. For further explanation we refer to Pacor *et al.* (2005) for DSM, and Gallovič and Brokešová (2007) for HIC.

Deterministic-Stochastic Method (DSM)

The DSM method is based on the well-known stochastic model of Boore (1983, 2003) but introduces two important modifications in order to consider the rupture propagation over a finite fault. First it uses a so-called deterministic envelope computed solving a simplified formulation of the representation theorem (Aki and Richards, 1980). The envelope is used for windowing the white Gaussian noise in the time domain. It is obtained by summing the contribution by each subfault in the order prescribed by isochrones (loci of points on the fault characterized by the same arrival time at the site). Through the isochrone calculation (Spudich and Frazier, 1984), the envelope depends on the rupture time over the fault and on the travel time through the crustal structure. This modification leads to a different ground-motion envelope at each site, instead of a predefined functional form as in the classical Boore's method. The second modification involves the definition of the reference omega-squared source spectrum that scales the windowed noise Fourier spectrum. In the DSM method the spectrum parameters are derived deterministically. The seismic moment of the target earthquake sets the low-frequency level of the spectrum while, for each site, the standard corner frequency is replaced by the apparent corner frequency defined as the inverse of the rupture duration as perceived at the site.

The definition of a deterministic envelope based on the isochrones theory and the use of an apparent corner frequency make the modeled synthetics particularly sensitive to the direction of rupture propagation over the fault with respect to the site position and, therefore, to the location of the rupture starting point. Indeed, sites in the forward rupture direction receive the energy from a larger portion of the fault in shorter time duration than the sites in the backward direction.

Despite these modifications, DSM still preserves the very simple nature of the stochastic model where only few

parameters need to be specified in the ground-motion calculation. However, it also presents some important limitations: its stochastic basis does not allow the modeling of near-fault long-period ground motion (especially for moderate and large earthquakes) where a pure deterministic calculation is more adequate; it accounts only for direct *S*-wave propagation, so that subsequent arrivals cannot be simulated; however, this is a reasonable assumption in the near-fault distance range where the direct-*S* wave field is generally dominant in amplitude with respect to *P* waves and secondary phases.

Hybrid-Integral-Composite Method (HIC)

For this more advanced kinematic technique, the rupture process is decomposed into slipping on individual overlapping subsources of various sizes, distributed randomly on the fault plane, treated differently in low- and high-frequency ranges. A database of the subsources is first created consisting of each subsource's dimension, position on the fault, mean slip (and consequently seismic moment), and corner frequency. The subsource number-size distribution obeys a power law with fractal dimension $D = 2$, and their mean slips are proportional to their dimensions (so-called constant stress-drop scaling, Zeng *et al.*, 1994). Note that this scaling implies that the subsources compose a *k*-squared slip distribution (Andrews, 1980). The same database of subsources is used for both the frequency ranges: in the low-frequency range (up to 2 Hz), the representation theorem is employed. The static slip at any point is given by the sum of the static slips of all the subsources containing the point (assuming a *k*-squared slip distribution at each individual subsource). The rupture time is computed considering the distance of the point from the nucleation point and constant rupture velocity V_r. The slip velocity function is assumed to be a Brune's pulse with constant rise time (1 sec). In this frequency range the directivity is well modeled. Concerning the high-frequency range (above 0.5 Hz), the subsources from the database are treated as individual point sources with Brune's source time function characterized by seismic moments and corner frequencies from the database. The rupture times are given by the time the rupture needs to reach the subsource's center (assuming the same constant rupture velocity V_r). The synthetics computed in the low- and high-frequency parts are crossover combined between 0.5 and 2 Hz in the Fourier domain by weighted averaging of the real and imaginary parts of the spectrum. The source modeling method is combined with the discrete-wavenumber method (Bouchon, 1981), yielding full-wave field Green's functions.

In our particular application to the Gubbio earthquake the strong-motion synthesis is mostly controlled by the composite (high frequency) approach as the minimum frequency considered is 0.25 Hz or 1 Hz (depending on the station, as previously described). Because of the random subsource positions, the wave-field contributions sum incoherently in the composite model, and the directivity effect is very weakly reproduced in the synthetics. It can be shown that the high-frequency plateau *A* of the acceleration spectrum (characterizing the strength of high-frequency radiation) is inversely proportional to the duration of the earthquake squared ($A \propto V_r^2/(LW)$; Aki, 1967). However, the constant of proportionality is unknown, being tightly related to the actual small-scale physical evolution of the rupture and has to be, therefore, considered as a free parameter. However, in principle, we are unable to distinguish in the high-frequency range the value of the rupture velocity V_r and the constant of proportionality. As suggested in Gallovič and Brokešová (2007), we initially compared synthetic PGAs with a regional ground-motion prediction equation (Bindi *et al.*, 2006) valid for the studied area. We set the constant of proportionality to 1, and we will understand the value of V_r in a more general sense as the combination of the rupture velocity and the constant of proportionality.

Simulation of the 1984 Gubbio Earthquake

Model Parameters Optimization

In this section we determine the scenario that produces minimum-misfit values for acceleration response spectra (5% damping) in order to infer information on the rupture kinematics of the event from the forward modeling of high-frequency strong-motion data. Considering that no previous studies (as waveform inversion analysis) are available to *a priori* constrain the position of the rupture starting point (N_p) and the value of the rupture velocity (V_r), we simulate several possible scenarios, varying the value of these two kinematic parameters within plausible ranges, in order to define the best source model that reproduces the 1984 earthquake records. We also used three different k^{-2} slip distributions on the fault (Herrero and Bernard, 1994; Gallovič and Brokešová, 2004) with the same average slip value (Table 1). The slip models are generated assuming a single asperity and varying its position over the fault plane (Fig. 2): in the slip model 1 the main asperity is located in the middle of the lower half of the fault, in slip model 2 the asperity has been moved toward the southeastern end of the fault, while in slip model 3 it is located close to the northwestern edge.

We looked for the best model only in terms of two kinematic parameters (N_p, V_r) and, therefore, we preferred to apply a simple grid-search method rather than any more complicated searching algorithm suitable for optimization in multidimensional parameter space. The grid search is performed by simulating 810 scenarios for each slip model combining different hypocenter positions and rupture velocity values over the fault. The search was performed using synthetics generated by both DSM and HIC techniques. We investigate 90 nucleation points (equally spaced by 0.5 km, see Fig. 2) and 9 rupture velocities (ranging from $0.6V_S$ to $1V_S$; $V_S = 3.3$ km/sec). The choice of considering only nucleation points located in the lower half of the fault is in accordance with the findings in Mai *et al.* (2005), in which

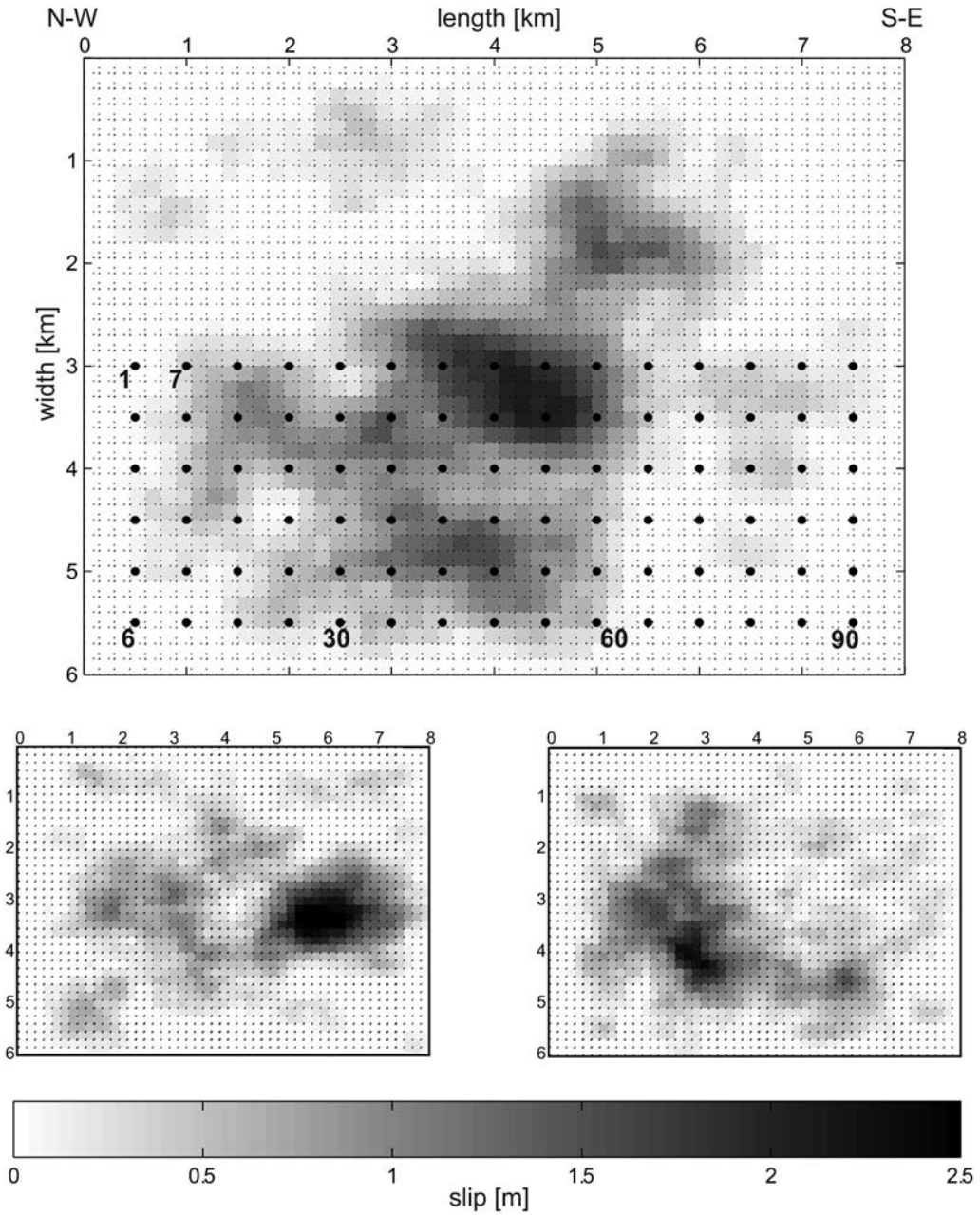

Figure 2. Fault geometry and the three k^{-2} final slip distributions adopted in the simulations. Black dots and labels show the position and number of nucleation points used in the grid search.

statistical analysis on a database of rupture models showed that rupture, in crustal earthquakes, tends to nucleate in the deeper sections of the fault.

To quantify the goodness of fit between synthetic and observed data, we define in the frequency domain an error function for each scenario as:

$$\varepsilon(N_p, V_r) = \frac{1}{m}\sum_{j=1}^{m} E_{\mathrm{rms}}(f_j), \tag{1}$$

where m is the number of the considered frequencies, N_p and V_r are the nucleation point and the rupture velocity of the considered scenario, respectively, and

$$E_{\mathrm{rms}}(f_j) = \left\{\frac{1}{n}\sum_{i=1}^{n}\left[\log\left(\frac{SA(f_j)_{\mathrm{obs}}}{SA(f_j)_{\mathrm{sim}}}\right)_i\right]^2\right\}^{1/2}, \tag{2}$$

with n as the number of stations and $SA(f)$ as the acceleration response spectra, 5% damped, computed at 34 selected frequencies in the band 1–9 Hz and for the mean between the horizontal components. Similar formulations have already been used in several studies (Graves and Pitarka, 2004; Castro and Ruíz-Cruz, 2005; Assatourians and Atkinson, 2007).

In order to account for the site amplification at the accelerometric stations, we multiply the Fourier amplitude

spectra of the synthetic time series computed at bedrock by the amplification function given by the HVSRs presented in the Source Model, Strong-Motion Data, and Site Effects section, obtaining ground-motion parameters at surface level.

The results of grid search for slip distribution 1 are shown in Figure 3. The upper panels show the values of ε for both modeling techniques. The best models (the absolute minimum of ε is about 0.17 and it is shown as a white star in Fig. 3) prefer rupture velocities around $0.9V_S$ (HIC best model) and $0.75V_S$ (DSM best model) with the nucleation point located close to the center of the fault for both methods ($N_p = 31$ and $N_p = 38$ for HIC and DSM best models, respectively). The pattern of the ε values shows that the HIC technique is more sensitive to the choice of rupture velocity. Scenarios with $\varepsilon < 0.20$ are obtained for $V_r > 0.8V_S$ but with a large number of hypocenter locations spanning almost all over the fault plane. The lower left-hand plot of Figure 3 shows the locations of nucleation points on the fault giving $\varepsilon < 0.2$ with a fixed $V_r = 0.9V_S$.

On the contrary, the right-hand panels of Figure 3 show that, adopting the DSM technique, scenarios with $\varepsilon < 0.2$ are obtained using a narrow range of V_r (from $0.7V_S$ to $0.8V_S$) and of nucleation point positions. Considering scenarios with $\varepsilon < 0.25$, the range of preferred V_r values increases (including almost all the considered values, depending on the hypocenter location) while the nucleation points remain constrained within an area around the center of the fault. Therefore, the choice of the position of rupture starting point seems to be of primary importance in the DSM modeling while it is secondary with respect to the choice of rupture velocity in HIC modeling. This behavior is strictly related to the different approach in simulating the rupture propagation on the fault adopted by the two techniques. As highlighted in the previous Methods section, DSM defines a deterministic envelope based on the computation of isochrones, which makes the technique especially sensitive to the position of the nucleation point. The HIC technique is, on the contrary, less sensitive to the nucleation point position (directivity) due to the incoherent summation of the subsource's contributions to the wave field in the high-frequency range.

The results of the grid search considering slip distribution 2 and 3 are not presented in the article because they are similar to those shown in Figure 3. The minimum ε values and their distribution in the space of possible solutions are

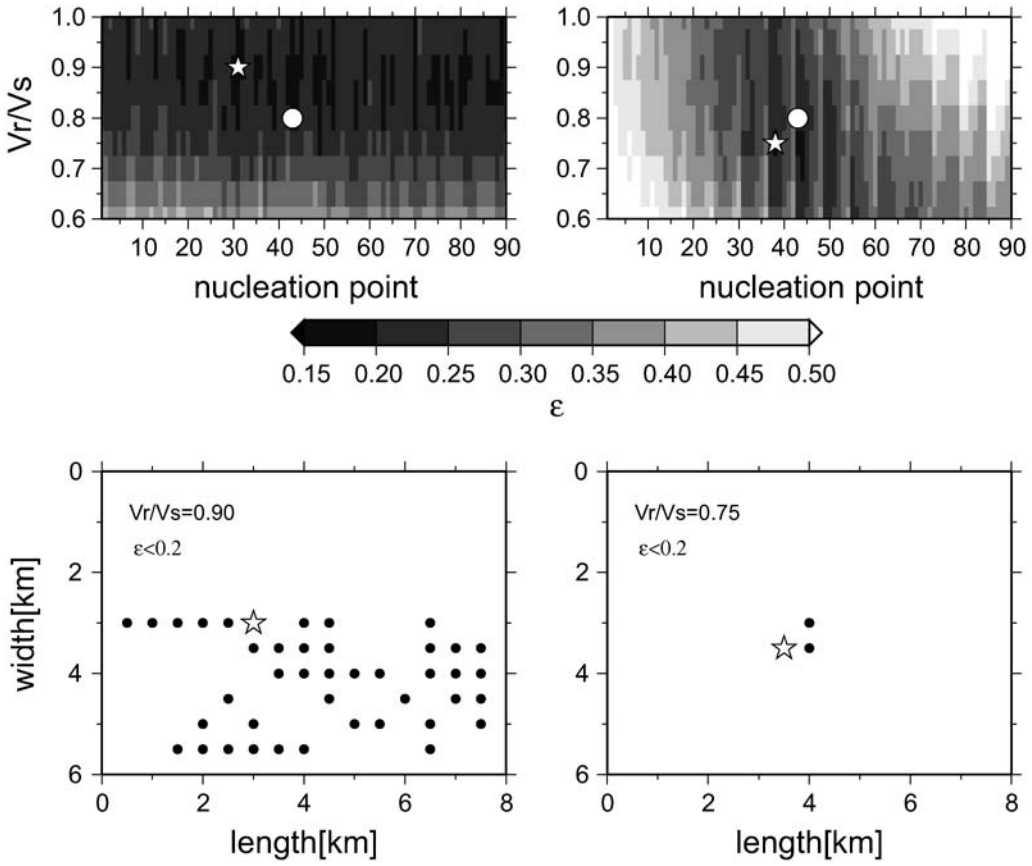

Figure 3. Grid-search results for HIC (left-hand plots) and DSM (right-hand plots) techniques. Upper panels: plots representing the value of ε as a function of the nucleation point (x axis) from 1 to 90 (see Fig. 2), and V_r/V_S values, that is, ratios of rupture velocity and shear-wave velocity (y axis), from 0.6 to 1.0. White stars correspond to the minimum values of ε, equal to 0.17 for both techniques, representing the best models. The unique best model is shown by the white dots. Lower panels: nucleation points (black dots) corresponding to a fixed V_r value (different for each technique and reported in the labels) for $\varepsilon < 0.20$ are represented on the fault plane.

consistent with those shown for slip model 1 (i.e., the rupture velocity is poorly constrained in DSM modeling while the hypocenter position is poorly constrained in HIC modeling). We conclude that, due to the moderate source dimension, the source–sites distances and the frequency band considered in the grid search, the goodness-of-fit estimator is sensitive predominantly to rupture velocity and nucleation point position and only loosely to the location of the main asperity of the slip model.

The grid search identifies two best models (one for each technique) presented in the lower panels of Figure 3. However, because a past earthquake corresponds to a single realization of all the possible rupture scenarios, we selected a unique best model that can reasonably represent the source kinematics of the 1984 Gubbio event. We searched for a single scenario that minimizes the ε function for both techniques, finding a hypocenter located at 4.0 km along strike and 3.0 km downdip ($N_p = 41$) and a rupture velocity equal to $0.8V_S$ (this unique model is represented in the top panels of Fig. 3 by a white dot). Slip distribution 1 is chosen, having no particular reason to prefer different dislocation models.

For each scenario, a model bias is obtained by averaging the residuals, that is, $\log_{10}(SA_{\text{obs}}/SA_{\text{sim}})$, among all stations at each frequency. Figure 4 presents the model bias for each technique considering the best models and the unique best model. A model bias of zero indicates that the simulation, on average, matches the observed ground-motion level. A negative model bias indicates overprediction of the observations and a positive model bias indicates underprediction of the observations. The best models have no significant bias over the frequency range from 1 to 9 Hz, with an average standard deviation of about 0.2, indicating that both simulation techniques are able to adequately capture the main characteristics of the ground-motion response. As expected, the unique best model gives worse results than the best models, leading to a slight underestimation for HIC simulations at frequencies higher than 4 Hz (Fig. 4a) and to overestimation for DSM synthetic at almost all frequencies (Fig. 4b).

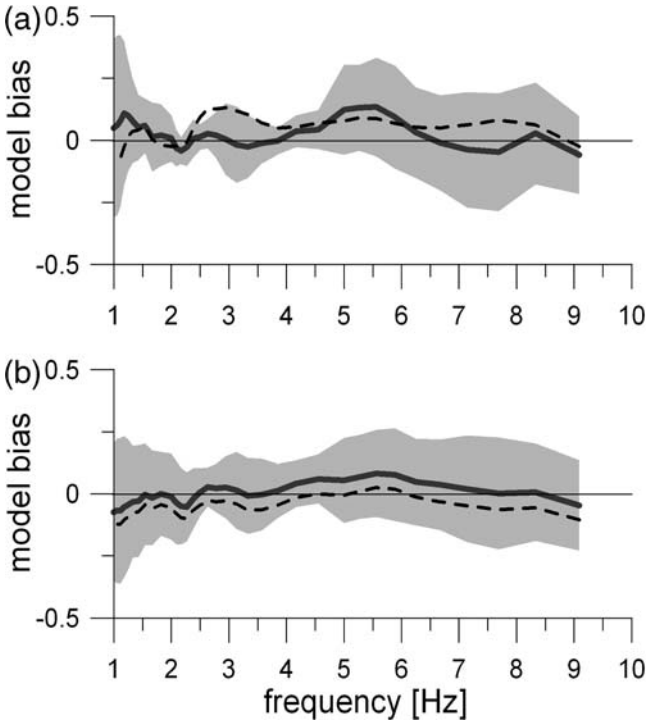

Figure 4. Spectral acceleration residuals ($\log_{10}(SA_{\text{obs}}/SA_{\text{sim}})$) as a function of frequency averaged over five sites and considering the best models for (a) HIC and (b) DSM techniques. The black curves and the light gray areas represent the median values and the standard deviations at each frequency, respectively. The median values considering the unique best model are also shown as a black dashed curve.

Comparison with Observed Data

As previously discussed, the adopted grid-search method is based on the comparison between observed and simulated acceleration response spectra in a restricted frequency range (1–9 Hz). In the following, we assess the reliability of the grid search results by more accurate comparisons between observed and synthetic ground motions for the selected source model.

Figure 5 shows the observed and simulated time series (both horizontal components) and acceleration response spectra (mean horizontal component) computed at the five stations, using the unique best model. The HIC method computes a time series very similar to the recorded ones, including *P* waves, *S* waves, and subsequent reverberations in the shallower crustal layers. NCR and CTC synthetic accelerograms match quite well with the recorded data, reproducing amplitudes and frequency content. The mismatch at PTL and UMB stations, mainly at frequencies higher than 4 Hz, could be ascribed both to radiation-pattern properties, because these sites are located close to the nodal planes for *S* waves, and to the approximated site amplification functions adopted in this study.

The waveforms obtained by the DSM method, accounting only for direct *S*-wave motion, appear to be much simpler than those observed and simulated by the HIC technique. However, the strong-motion phase is well reproduced, providing consistent results in terms of ground-motion parameters. The DSM response spectra match quite well with the data recorded at the NCR and UMB stations, while results similar to those obtained by the HIC method are found for data recorded at the PTL site, confirming the presence of peculiar site effects not accounted for in the HVSR function. An overestimation is visible at the CTC and GBB sites for frequencies greater than 6 Hz; however, the fits improve if a higher rupture velocity is adopted, as found from the grid-search analysis.

To quantify the comparison presented in Figure 5 we compute residuals for several ground-motion parameters usually required in engineering analysis (Fig. 6). We considered two instantaneous measures of motion (PGA and PGV) and three integral measures (HI, AI, and T90). T90 is defined

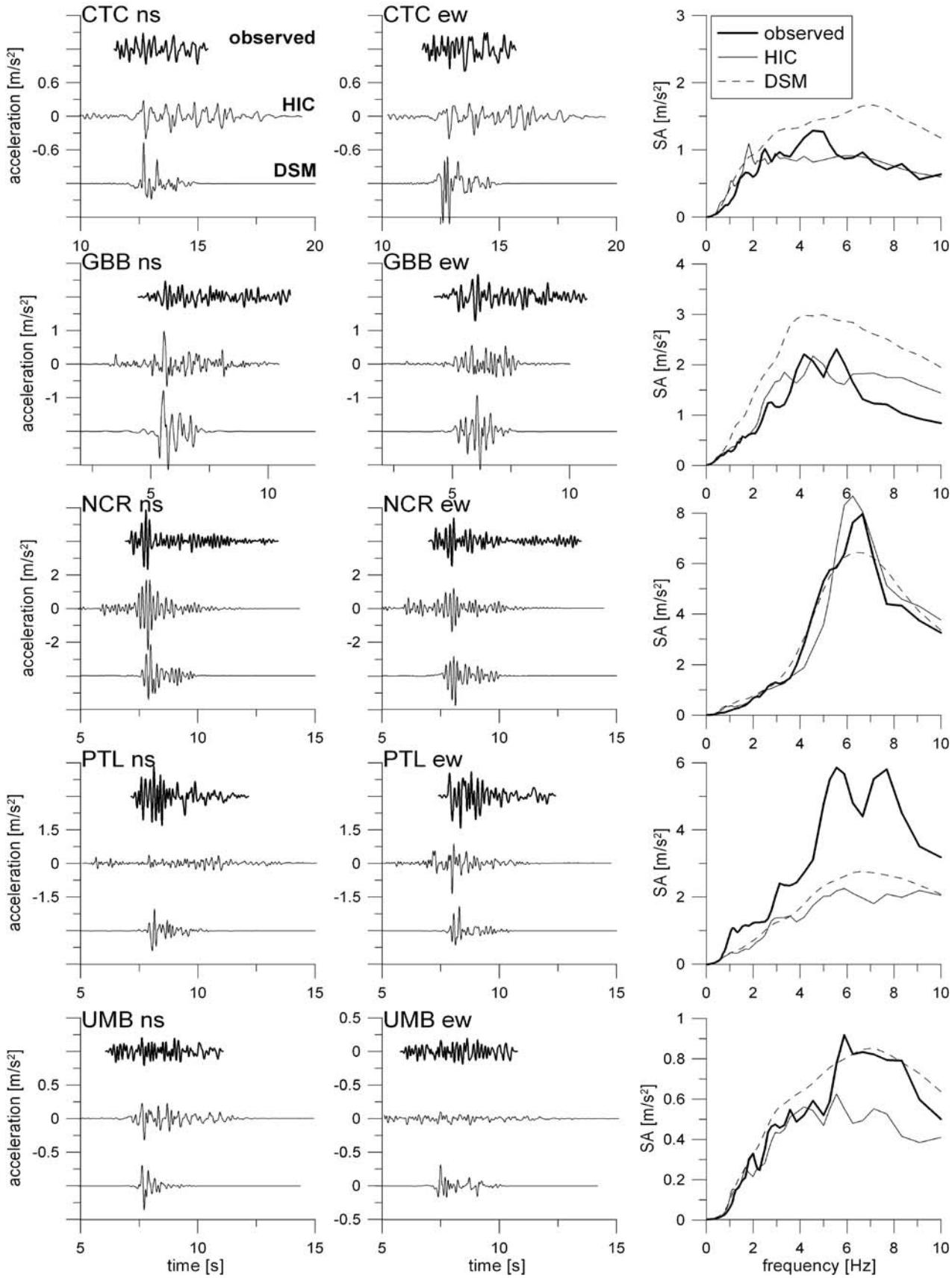

Figure 5. Comparison between observed (*S*-wave time window) and simulated time series (north–south and east–west component) and 5% damped acceleration response spectra (mean horizontal component) at the five stations and for both simulation techniques.

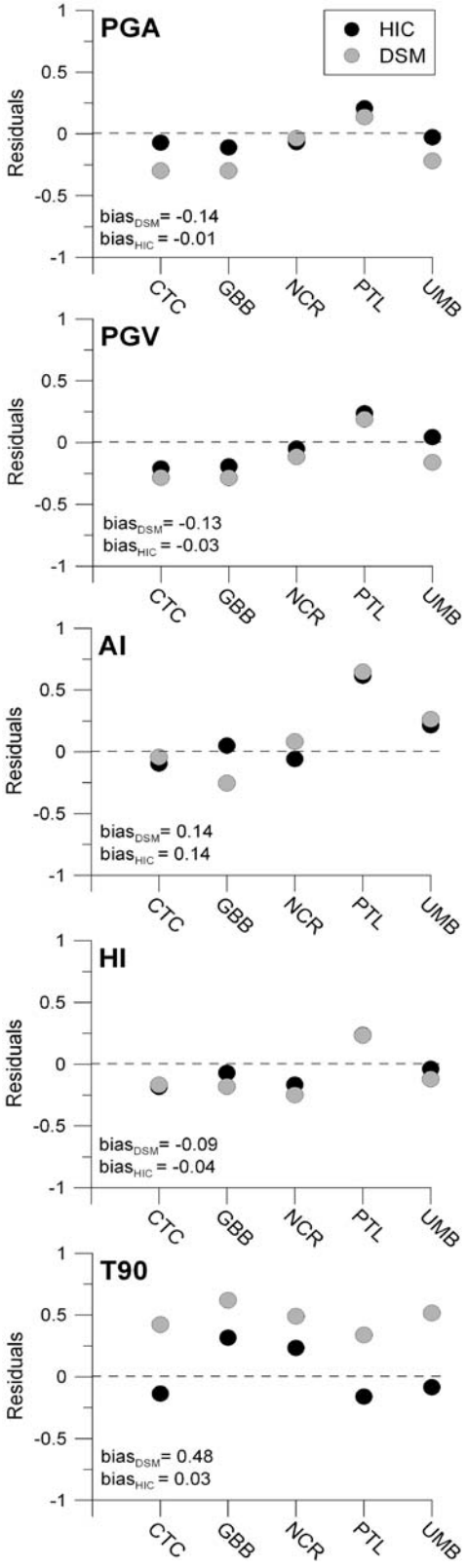

Figure 6. Residuals computed for different ground-motion parameters (mean horizontal component) at each station. Black and gray dots represent residuals computed using the HIC and DSM unique best model, respectively (see Fig. 3). For each parameter, the given model bias is computed by averaging the residuals over all the stations.

as the time interval between 5% and 95% of the cumulative square of the acceleration time history (Husid, 1969). All the parameters are computed from the time series filtered as described in the previous section. A model bias for each technique is also calculated averaging the residuals over the five stations. The synthetic peak values well reproduce the observed ones, and the residuals from both techniques are quite consistent. At CTC and GBB sites the overestimation of the high-frequency content of the observed spectra in the DSM synthetics produces larger PGA residuals (in any case not exceeding a factor of 2). Regarding AI and HI, both techniques provide comparable results and reproduce fairly well the observed parameters, particularly a lower bias is found for HI. At the PTL station, HIC and DSM underestimate the observed AI (by about a factor of 3), likely due to the aforementioned improper site response applied to the synthetics. DSM also overestimates the AI at the GBB site, related to the high-frequency content in the synthetic acceleration time series. DSM produces high-positive residuals for T90 with model bias equal to 0.48 indicating that the duration of observed strong motion cannot be captured by this technique. In fact DSM, simulating only the strong-motion phase of the seismogram, is able to reproduce the cumulative energy but it results in being contained in a too short and not realistic time duration.

Variability of Ground-Motion Parameters

Typically when computing ground-motion scenarios we are not able to compare results with observed data to calibrate, as discussed previously, the kinematic parameters of the model. The aleatory variability of these parameters can strongly affect the prediction of ground-motion values (Sørensen *et al.*, 2007). The choice of a particular rupture nucleation point could lead, for instance, to increasing PGA values with a consequent increasing hazard or loss estimate for a particular area (Ameri *et al.*, 2008, Ansal *et al.*, 2008). Furthermore, the variability of PGA values, associated with the specific choice of the kinematic parameters, could be different with respect to the variability of other parameters, such as AI, T90, or HI.

To investigate and quantify this variability as a function of the source kinematics, we compute the residuals for the different ground-motion parameters from the more than 2400 scenarios simulated, combining 6 rupture velocities, 90 nucleation points, and 3 slip distributions. The residuals at each station and for both techniques are presented in Figure 7 and in Table 4.

For both techniques and for all sites, the standard deviations of the residuals distributions for different ground-motion parameters are remarkably different. The AI residuals are characterized by the largest standard deviation (almost twice as large compared to the PGA and PGV ones). On the contrary, T90s have the lowest values of standard deviation, meaning a narrow range of predicted values: for instance, at the NCR site, about 68% of the T90 values from HIC syn-

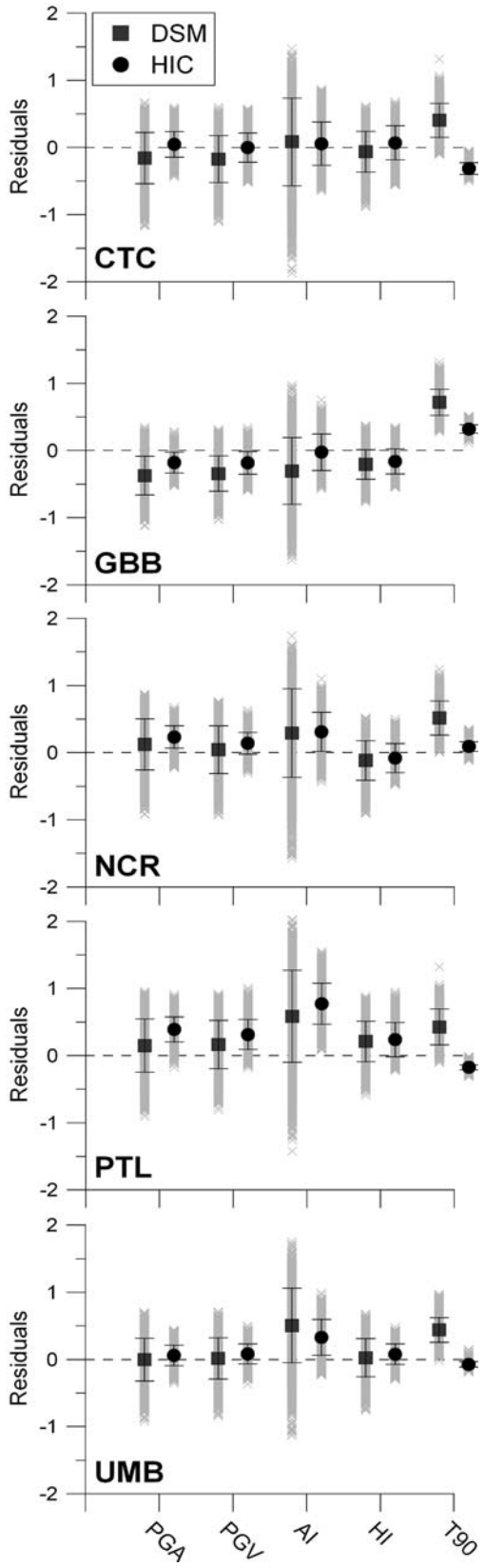

Figure 7. Residuals for all the 2430 scenarios, considering different ground-motion parameters at the five stations (gray crosses). The mean and standard deviation of the residuals distributions are shown for both modeling techniques (see also Table 4).

Table 4
Mean and Standard Deviation of the Residual Distributions at All Stations*

Station Name	DSM	HIC
	PGA	
CTC	−0.16 ± 0.38	0.05 ± 0.19
GBB	−0.37 ± 0.29	−0.18 ± 0.16
NCR	0.12 ± 0.38	0.23 ± 0.17
PTL	0.15 ± 0.40	0.39 ± 0.19
UMB	−0.01 ± 0.32	0.06 ± 0.15
	PGV	
CTC	0.09 ± 0.35	0.26 ± 0.22
GBB	−0.34 ± 0.26	−0.18 ± 0.17
NCR	0.04 ± 0.35	0.14 ± 0.16
PTL	0.17 ± 0.36	0.31 ± 0.22
UMB	0.02 ± 0.31	0.08 ± 0.15
	AI	
CTC	0.08 ± 0.65	0.06 ± 0.32
GBB	−0.30 ± 0.50	−0.03 ± 0.27
NCR	0.29 ± 0.66	0.31 ± 0.29
PTL	0.58 ± 0.68	0.77 ± 0.31
UMB	0.51 ± 0.55	0.33 ± 0.27
	HI	
CTC	−0.06 ± 0.30	0.07 ± 0.25
GBB	−0.21 ± 0.22	−0.16 ± 0.19
NCR	−0.12 ± 0.30	−0.08 ± 0.21
PTL	0.21 ± 0.30	0.24 ± 0.26
UMB	0.03 ± 0.28	0.08 ± 0.15
	T90	
CTC	0.40 ± 0.25	−0.31 ± 0.09
GBB	0.72 ± 0.19	0.32 ± 0.06
NCR	0.52 ± 0.25	0.09 ± 0.07
PTL	0.43 ± 0.27	−0.18 ± 0.04
UMB	0.44 ± 0.18	−0.07 ± 0.04

See Figure 7 also.
*Results are presented for each ground-motion parameter considering both simulation methods.

thetics are distributed in a range of 1 sec. PGA, PGV, and HI residuals present quite similar distributions with standard deviation included between the previous two. Other studies based both on recorded data (Abrahamson and Silva, 1996; Travasarou *et al.*, 2003; Massa *et al.*, 2008) and simulations from dynamic rupture models (Aochi and Douglas, 2006) have confirmed that the standard deviation associated with AI and T90 are larger and smaller, respectively, than that of most other ground-motion parameters. AI is proportional to the integral of the squared acceleration time series. As a consequence, this measure accounts for the effect of both the acceleration amplitude (squared) and the duration of motion. Therefore, it is expected to have a higher variability of AI with respect to the PGA although the variations of the model input parameters are the same. T90, in the absence of particular response site (e.g., basin effects) that could lead to large increase of signal's duration, depends primarily on the travel time through the crustal model (that is fixed for each station) and depends secondarily on the rupture duration. The latter is related to the fault-plane dimension (fixed) and to the

combination of nucleation point position and rupture velocity (variable). Thus, the variability of simulated T90 is mainly constrained by the small dimension of the considered causative fault.

Table 4 also shows that the value of standard deviation is station dependent. Although we considered only five sites, it is noteworthy that observers located approximately in the fault-parallel direction (CTC, NCR, and PTL) present larger dispersion (i.e., standard deviation) of the residuals with respect to sites located in fault-normal direction (GBB and UMB). This larger standard deviation is due to forward and backward directivity that increase the variability for certain sites.

The standard deviations of the residual distributions for HIC modeling are systematically smaller than those of DSM modeling. However, the mean values obtained by both techniques are consistent within the statistical error, except for the T90 (Fig. 7). The differences in the mean values of T90 distributions between the two simulation methods are consistent with the differences highlighted in Figure 6 for the best model.

As already discussed, the different variability between DSM and HIC results is related to the different numerical description of the extended source. Firstly, the HIC method is less sensitive to the choice of the location of nucleation points than DSM as found by the grid-search analysis; secondly, the HIC method is sensitive to the slip distribution because the low-frequency content of the ground motion is computed deterministically; however, the analyzed parameters are mainly controlled by the higher frequencies. Moreover, in the considered source–site distance range (from about 18 to 38 km) the effect of different slip distributions on the ground motion is not significant.

In summary, the differences in the residuals distributions related to the variability of the kinematic parameters are visible for both methods and at all sites and have important implications for prediction of ground motion from future events. For example, the standard deviation for the T90 residuals at the GBB station calculated with the HIC technique is 0.06; this means that, despite the large variability of the kinematic parameters, the variability in T90 is very small. On the contrary, AI residuals show the largest dispersion (especially with the DSM technique, $\sigma = 0.50$ at the GBB site), thus, in blind ground-motion prediction, we have to take into account that this parameter could be very sensitive to the variation of kinematic parameters.

Discussion and Conclusions

In the first part of the article we focused our attention on the modeling of the 1984 M_w 5.7 Gubbio earthquake at five accelerometric stations. After taking approximate corrections for site effects into account, we searched for optimal values of the free kinematic parameters considered in the study (i.e., the rupture velocity and the hypocenter position) by minimizing a misfit function expressed in terms of acceleration response spectra in order to infer the best scenario to fit the data.

We hypothesized 90 nucleation points located in the lower half of the fault and 9 rupture velocities (ranging from 0.6 to $1V_S$) and investigated all the possible combinations of these parameters. Moreover, we considered three different k^{-2} slip distributions over the fault moving the position of the main asperity.

We computed synthetic seismograms using two simulation techniques, the DSM (Pacor *et al.*, 2005) and the HIC (Gallovič and Brokešová, 2007), the former being able to reproduce high-frequency synthetic seismograms ($f >$ 0.5 Hz) accounting for the propagation of direct S waves and the latter being a more advanced technique able to produce full-wave-field broadband synthetics. The results provide some insight into the rupture process of the event based on high-frequency information in the observed data. In principle, the DSM method is capable of constraining both the nucleation point position and the rupture velocity as its synthetics are sensitive directly to these features. On the contrary, the HIC method provides synthetics only loosely sensitive to the directivity and generalized rupture velocity.

Based on joint results from both modeling methods, we found that the most probable nucleation point of the 1984 earthquake was located in an area around the center of the fault (see Fig. 3) resulting in a bilateral rupture propagating with a velocity close to 2.65 km/sec. Because of the moderate dimension of the source, the distances to the recording stations, and the frequency range considered in the grid search, the results are not substantially affected by the slip patch distribution. We want to point out that such results are not provided by inversion of recorded data but simply by minimizing the acceleration response spectra residuals from all the plausible scenarios simulated with both techniques. Although the few number of available stations represents a limit of the proposed approach, we are confident that their good azimuthal coverage (that constrain the hypocenter position on the fault) and their proximity to the source allow a reliable first estimation of the kinematics of Gubbio earthquake.

The modeling of the 1984 event allowed also to assess the capability of the adopted techniques to reproduce earthquake ground-motion parameters usually required in engineering analysis. Both modeling approaches have no significant spectral acceleration bias over the frequency range from 1 to 9 Hz, indicating that the simulation models adequately capture the main characteristics of the ground motion. Considering other commonly used strong-motion parameters we found that the peak values (acceleration and velocity), AI, and HI are well modeled by both simulation techniques. The HIC method appears to be the most complete technique providing lower model bias values and being able to reproduce, on average, also the duration of motion; on the contrary DSM failed in reproducing realistic time-series durations. Among the considered integral measures of ground

motion, HI turns out to be best reproduced by both simulation techniques, while AI seems to be the most difficult to model. It is particularly important, when performing scenario studies, to assess the capability of different simulation techniques to reproduce several ground-motion parameters, so we could be able to recognize *a priori* which simulation method is more suitable for a specific purpose. In this case DSM is able to adequately reproduce PGA, PGV, spectral acceleration, and HI with the advantage of requiring approximately half the computational time and a smaller number of input parameters than the HIC method. However, this latter technique is more appropriate when a correct evaluation of the duration of the ground shaking is required.

In the second part of the article we analyze all the scenarios produced for the 1984 earthquake fault to quantify how the variation of simulated strong-motion parameters is related to the variability (i.e., uncertainties) of the kinematic parameters of the model.

We study the residuals distribution of the five strong-motion parameters considered in this study, and we investigate two types of variability. The first variability depends on the modeling approach: the variances of the DSM synthetics distributions are systematically higher than the HIC ones. The second variability is related to the predicted strong-motion parameter: AI presents the widest distribution (highest standard deviation) while T90 presents the most narrow distribution (lowest standard deviation). PGA, PGV, and HI present similar distribution with standard deviation values between the two previously mentioned. These results are verified considering all the computed strong-motion parameters and at all the selected stations.

The standard deviations of residuals distributions also depend on the position of the site with respect to the extended fault. Stations located in the fault-parallel direction present larger standard deviations with respect to sites located in fault-normal direction. Although the reliability of this result is limited in the present study by the few number of available sites, it is consistent with the results of Ripperger *et al.* (2008) on the variability of PGV from dynamic rupture simulations performed assuming a heterogeneous initial stress field.

In order to better understand how uncertainties of different kinematic parameters for both simulation techniques contribute to variability of ground motion, Figure 8 shows the synthetic cumulative distribution functions (CDFs) computed at the GBB and NCR sites for PGV. In Figure 8a, the three CDFs are related to each slip model: we grouped the scenarios with a fixed slip model and variable nucleation point position and rupture velocity, obtaining a total number of 810 realizations. In Figure 8b the CDFs are calculated for three different rupture velocities ($0.6V_S$, $0.8V_S$, and $1V_S$) for a total number of 270 scenarios for each V_r (3 slip models, 1 rupture velocity, and 90 nucleation points). In Figure 8c the scenarios are grouped considering three nucleation areas containing 30 hypocenters each for a total of 810 scenarios (3 slip models, 9 rupture velocities, and 30 nucleations). We note that the choice of a particular slip distribution has a minimum influence in the ground-motion distribution (Fig. 8a). On the other hand, the variation of rupture velocity and nucleation point largely contributes to variability of ground motion. The CDFs in Figure 8b are shifted to larger PGV values as the selected V_r increases. The effect of the nucleation area (Fig. 8c) is more complicated being dependent on the position of the site; for instance, at the GBB site, nucleation areas 2 and 3 produce very similar PGV distributions. In general uncertainties in the hypocenter position produce a variability of ground motion of the same order or smaller than uncertainties in rupture velocity for the HIC method and of the same order or larger for DSM.

These results have important implications for ground-motion prediction. If we are interested in calculating, for instance, AI for a hypothetical earthquake scenario, we have to take into account that this parameter is very sensitive to the variability of kinematic parameters. Choosing a different value of rupture velocity or a different position of the nucleation point will affect the predicted AI more than the HI or PGA. Moreover, in the case of the considered earthquake and distance range, uncertainties in the slip model definition can be considered negligible while larger contribution to ground-motion variability is given by uncertainties in nucleation point location and rupture velocity. In other words, considering a single slip model (e.g., slip model 1) we would not significantly underestimate the variability of ground motion from a larger number of slip models.

Commonly, AIs and HIs are assumed to be closely related to the damage potential of an earthquake. The results of this study show that HI is the best modeled among the considered integral measures, the values provided by both simulation methods are highly consistent, and its variability is less affected by the lack of knowledge in the source kinematic properties (lower standard deviation). For these reasons HI should be preferred for evaluating, through the use of synthetic seismograms, the seismic response of structures subject to a hypothetical earthquake.

Finally, we highlight that, by computing several possible scenarios at each site, we produce synthetic probability distributions of engineering ground-motion parameters, which allow one to estimate every statistical quantity (e.g., median, maximum, percentiles, etc.) engineers would need for defining the seismic input in structural engineering or hazard studies.

Data and Resources

Seismograms recorded during the 1984 Gubbio earthquake used in this study can be obtained from the database of the Italian strong-motion data (Working Group Italian Accelerometric Archive [ITACA]) at http://itaca.mi.ingv.it (last accessed September 2008).

The causative fault of the 1984 earthquake is reported in the Database of Individual Seismogenic Sources (DISS), Version 3.0.4: A Compilation of Potential Sources for Earth-

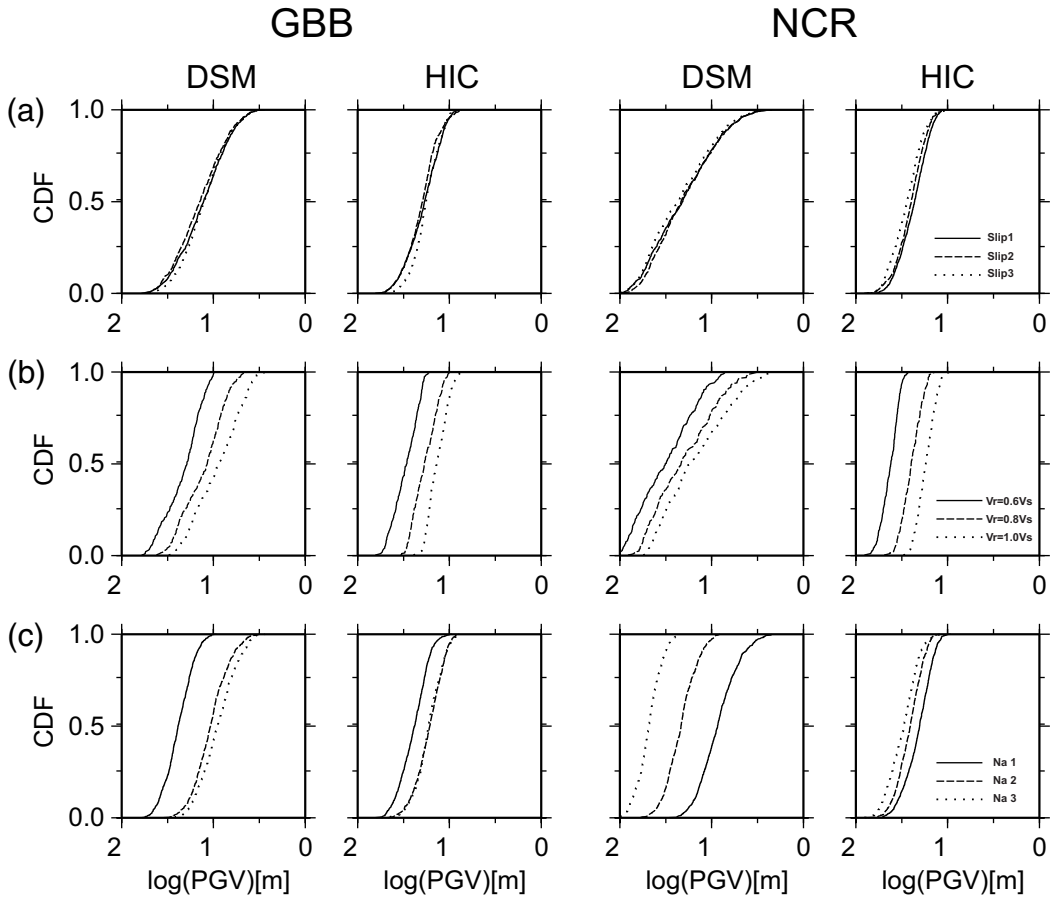

Figure 8. PGV synthetic CDFs computed at GBB and NCR stations for both techniques. (a) Each CDF is computed grouping scenarios that share the same slip model (810 scenarios for each slip model). (b) Each CDF is computed grouping scenarios that share the same rupture velocity (V_r) considering three selected values. (c) Each CDF is computed grouping scenarios that share the same rupture nucleation area (Na); for example, Na 1 contains nucleation points from 1 to 30 in Figure 2.

quakes Larger than M 5.5 in Italy and Surrounding Areas, available at http://www.ingv.it/DISS/, last accessed September 2008 (© INGV 2007; DISS Working Group, 2007; Basili *et al.*, 2007).

Some plots were made using the Generic Mapping Tools version 3.3.6 (Wessel and Smith, 1998; www.soest.hawaii.edu/gmt, last accessed September 2008).

Acknowledgments

This work was performed within the project titled S3–Shaking and damage scenarios in area of strategic and/or priority interest, supported by the Italian Civil Protection (DPC) and the Istituto Nazionale di Geofisica e Vulcanologia (INGV) for the time span of 2004–2007.

The manuscript has greatly benefited from careful review and comments of Karen Assatourians, Associate Editor Gail Atkinson, and an anonymous reviewer. We thank Sara Lovati and Lucia Luzi for providing information on site response in the area. Roberto Basili provided the fault parameters for the 1984 Gubbio earthquake. We particularly thank Paul Spudich and Dino Bindi for providing fruitful comments on an early version of the manuscript.

Gabriele Ameri carried out this work as a Ph.D. student of the Dipartimento per lo Studio del Territorio e delle sue Risorse, University of Genoa, Italy.

František Gallovič has been supported by the Grant Agency of the Czech Republic (Grant Number 205/08/P013) and Grant Number MSM0021620800 and by the Dipartimento di Scienze Fisiche, University "Federico II", Naples. Italy.

References

Abrahamson, N. A., and W. J. Silva (1996). Empirical ground motion models, report to Brookhaven National Laboratory.

Aki, K. (1967). Scaling law of seismic spectrum, *J. Geophys. Res.* **72,** 1217–1231.

Aki, K., and P. G. Richards (1980). *Quantitative Seismology: Theory and Methods*, Vol. **1** and **2,** W. H. Freeman, San Francisco, 932 pp.

Ameri, G., F. Pacor, G. Cultrera, and G. Franceschina (2008). Deterministic ground-motion scenarios for engineering applications: the case of Thessaloniki, Greece, *Bull. Seismol. Soc. Am.* **98,** no. 3, 1289–1303.

Andrews, D. J. (1980). A stochastic fault model, 1, static case, *J. Geophys. Res.* **85,** 3867–3877.

Ansal, A., A. Akinci, G. Cultrera, M. Erdik, V. Pessina, G. Tonuk, and G. Ameri (2008). Loss estimation in Istanbul based on deterministic earthquake scenarios of the Marmara Sea region (Turkey), *Soil Dyn. Earthq. Eng.* (in press).

Aochi, H., and J. Douglas (2006). Testing the validity of simulated strong ground motion from the dynamic rupture of a finite fault, by using empirical equations, *Bull. Earthq. Eng.* **4,** 211–229, doi 10.1007/s10518-006-0001-3.

Archuleta, R. J., and S. H. Hartzell (1981). Effects of fault finiteness on near-source ground motion, *Bull. Seismol. Soc. Am.* **71,** 939–957.

Assatourians, K., and G. M. Atkinson (2007). Modeling variable-stress distribution with the stochastic finite-fault technique, *Bull. Seismol. Soc. Am.* **97,** 1935–1949.

Basili, R., G. Valensise, P. Vannoli, P. Burrato, U. Fracassi, S. Mariano, M. M. Tiberti, and E. Boschi (2007). The database of individual seismogenic sources (DISS), version 3: summarizing 20 years of research on Italy's earthquake geology, *Tectonophysics* **453,** 20–43.

Bindi, D., R. R. Castro, G. Franceschina, L. Luzi, and F. Pacor (2004). The 1997–1998 Umbria-Marche sequence (central Italy): source, path, and site effects estimated from strong motion data recorded in the epicentral area, *J. Geophys. Res.* **109,** B04312, doi 10.1029/2003JB002857.

Bindi, D., L. Luzi, F. Pacor, G. Franceschina, and R. R. Castro (2006). Ground-motion predictions from empirical attenuation relationships versus recorded data: the case of the 1997–1998 Umbria-Marche, central Italy, strong-motion data set, *Bull. Seismol. Soc. Am.* **96,** no. 3, 984–1002.

Bommer, J. J., and A. B. Acevedo (2004). The use of real earthquake accelerograms as input to dynamic analysis, *J. Earthq. Eng.* **8,** no. S1, 43–92.

Boore, D. M. (1983). Stochastic simulation of high-frequency ground motion based on seismological models of the radiated spectra, *Bull. Seismol. Soc. Am.* **73,** 1865–1894.

Boore, D. M. (2003). Simulation of ground motion using the stochastic method, *Pure Appl. Geophys.* **160,** 635–676.

Bordoni, P., G. Cultrera., L. Margheriti, P. Augliera, G. Caielli, M. Cattaneo, R. De Franco, A. Michelini, and D. Spallarossa (2003). A microseismic study in a low seismicity area: the 2001 site-response experiment in the Città di Castello Basin (Italy), *Ann. Geophys.* **46,** no. 6, 1345–1360.

Bouchon, M. (1981). A simple method to calculate Green's functions for elastic layered media, *Bull. Seismol. Soc. Am.* **71,** 959–971.

Castro, R. R., and E. Ruíz-Cruz (2005). Stochastic modeling of the 30 September 1999 M_w 7.5 earthquake, Oaxaca, Mexico, *Bull. Seismol. Soc. Am.* **95,** no. 6, 2259–2271.

Castro, R. R., F. Pacor, D. Bindi, G. Franceschina, and L. Luzi (2004). Site response of strong motion stations in the Umbria, central Italy, region, *Bull. Seismol. Soc. Am.* **94,** no. 2, 576–590.

Cattaneo, M., and A. Marcellini. (2000). Terremoto dell'Umbria-Marche: analisi della sismicita' recente dell'appennino umbro-marchigiano—microzonazione sismica di Nocera Umbra e Sellano, (CNR-Gruppo Nazionale per la Difesa dai Terremoti, Roma).

Cultrera, G., A. Rovelli, G. Mele, R. Azzara, A. Caserta, and F. Marra (2003). Azimuth dependent amplification of weak and strong ground motions within a fault zone (Nocera Umbra, central Italy), *J. Geophys. Res.* **108,** no. B3, 2156, doi 10.1029/2002JB001929.

Douglas, J. (2003). Earthquake ground motion estimation using strong-motion records: a review of equations for the estimation of peak ground acceleration and response spectral ordinates, *Earth Sci. Rev.* **61,** no. 1–2, 43–104.

Field, E. H., and K. H. Jacob (1995). A comparison and test of various site-response estimation techniques, including three that are not reference-site dependent, *Bull. Seismol. Soc. Am.* **85,** 1127–1143.

Gallovič, F., and J. Brokešová (2004). The k^{-2} rupture model parametric study: example of the 1999 Athens earthquake, *Studia Geoph. Geod.* **48,** 589–613.

Gallovič, F., and J. Brokešová (2007). Hybrid *k*-squared source model for strong ground motion simulations: introduction, *Phys. Earth Planet. Interiors* **160,** 34–50.

Graves, R., and A. Pitarka (2004). Broadband time history simulation using a hybrid approach, *Proc. of 13th World Conf. on Earthquake Engineering*, Vancouver, British Columbia, 1–6 August 2004.

Hanks, T. C., and H. Kanamori (1979). A moment-magnitude scale, *J. Geophys. Res.* **84,** 2348–2350.

Hartzell, S., M. Guatteri, P. M. Mai, P. Liu, and M. Fisk (2005). Calculation of broadband time histories of ground motion, part II: kinematic and dynamic modeling using theoretical Green's functions and comparison with the 1994 Northridge earthquake, *Bull. Seismol. Soc. Am.* **95,** 614–645.

Herrero, A., and P. Bernard (1994). A kinematic self-similar rupture process for earthquakes, *Bull. Seismol. Soc. Am.* **84,** 1216–1228.

Husid, R. L. (1969). Analisis de terremotos: analisis general, *Revista del IDIEM* **8,** 21–42, Santiago, Chile.

Iervolino, I., and C. A. Cornell (2005). Record selection for nonlinear seismic analysis of structures, *Earthq. Spectra* **21,** no. 3, 685–713.

Lermo, J., and F. J. Chávez-García (1993). Site effect evaluation using spectral ratios with only one station, *Bull. Seismol. Soc. Am.* **83,** 1574–1594.

Liu, P., R. J. Archuleta, and S. H. Hartzell (2006). Prediction of broadband ground-motion time histories: hybrid low/high-frequency method with correlated random source parameters, *Bull. Seismol. Soc. Am.* **96,** no. 6, 2118–2130.

Luzi, L., D. Bindi, G. Franceschina, F. Pacor, and R. R. Castro (2005). Geotechnical site characterisation in the Umbria Marche area and evaluation of earthquake site-response, *Pure Appl. Geophys.* **162,** 2133–2161.

Mai, P. M., P. Spudich, and J. Boatwright (2005). Hypocenter locations in finite-source rupture models, *Bull. Seismol. Soc. Am.* **95,** no. 3, 965–980.

Malagnini, L., and R. B. Herrmann (2000). Ground-motion scaling in the region of the 1997 Umbria-Marche earthquake (Italy), *Bull. Seismol. Soc. Am.* **90,** 1041–1051.

Marra, F., R. Azzara, F. Bellucci, A. Caserta, G. Cultrera, G. Mele, B. Palombo, A. Rovelli, and E. Boschi (2000). Large amplification of ground motion at rock sites within a fault zone in Nocera Umbra (central Italy), *J. Seism.* **4,** 543–554.

Massa, M., P. Morasca, L. Moratto, S. Marzorati, G. Costa, and D. Spallarossa (2008). Empirical ground motion prediction equations for northern Italy using weak and strong motion amplitudes, frequency content and duration parameters, *Bull. Seismol. Soc. Am.* **98,** 1319–1342.

Mirabella, F., M. G. Ciaccio, M. R. Barchi, and S. Merlin (2004). The Gubbio Normal fault (central Italy): geometry, displacement distribution and tectonic evolution, *J. Struct. Geol.* **26,** 2233–2249.

Pacor, F., D. Bindi, L. Luzi, S. Parolai, S. Marzorati, and G. Monachesi (2007). Characteristics of strong ground motion data recorded in the Gubbio sedimentary basin (central Italy), *Bull. Earthq. Eng.* **5,** 27–43, doi 10.1007/s10518-006-9026-x.

Pacor, F., G. Cultrera, A. Mendez, and M. Cocco (2005). Finite fault modeling of strong ground motions using a hybrid deterministic–stochastic approach, *Bull. Seismol. Soc. Am.* **95,** no. 1, 225–240.

Pavic, R., M. G. Koller, P.-Y. Bard, and C. Lacave-Lachet (2000). Ground motion prediction with the empirical Green's function technique: an assessment of uncertainties and confidence level, *J. Seism.* **4,** 59–77.

Pucci, S., P. M. De Martini, D. Pantosti, and G. Valensise (2003). Geomorphology of the Gubbio Basin (central Italy): understanding the active tectonics and earthquake potential, *Ann. Geophys.* **46,** no. 5, 837–864.

Ripperger, J., P. M. Mai, and J.-P. Ampuero (2008). Variability of near-field ground motion from dynamic earthquake rupture simulations, *Bull. Seismol. Soc. Am.* **92,** 2217–2232.

Rovelli, A., A. Caserta, F. Marra, and V. Ruggiero (2002). Can seismic waves be trapped inside an inactive fault zone? The case study of Nocera Umbra, central Italy, *Bull. Seismol. Soc. Am.* **92,** 2217–2232.

S3 Project (2007). Scenari di scuotimento in aree di interesse prioritario e/o strategico. Deliverable D20: bedrock shaking scenarios: available at http://esse3.mi.ingv.it/deliverables/Deliverables_S3_D20.pdf.

Shakal, A., H. Haddadi, V. Graizer, K. Lin, and M. Huang (2006). Some key features of the strong-motion data from the **M** 6.0 Parkfield, California, earthquake of 28 September 2004, *Bull. Seismol. Soc. Am.* **96,** no. 4b, S90–S118.

Somerville, P. G., N. F. Smith, R. W. Graves, and N. A. Abrahamson (1997). Modification of empirical strong ground motion attenuation relations to include the amplitude and duration effects of rupture directivity, *Seism. Res. Lett.* **68,** 199–222.

Sørensen, M. B., N. Pulido, and K. Atakan (2007). Sensitivity of ground-motion simulations to earthquake source parameters: a case study for Istanbul, Turkey, *Bull. Seismol. Soc. Am.* **97,** no. 3, 881–900.

Spudich, P., and L. N. Frazer (1984). Use of ray theory to calculate high-frequency radiation from earthquake sources having spatially variable rupture velocity and stress drop, *Bull. Seismol. Soc. Am.* **74,** 2061–2082.

Stewart, J. P., S. J. Chiou, J. D. Bray, R. W. Graves, P. G. Somerville, and N. A. Abrahamson (2001). Ground motion evaluation procedures for performance-based design, Pacific Earthquake Engineering Research (PEER) Center Report 2001/09, University of California, Berkeley.

Travasarou, T., J. D. Bray, and N. A. Abrahamson (2003). Empirical attenuation relationship for Arias Intensity, *Earth. Eng. Struct. Dyn.* **32,** no. 7, 1133–1155.

Wang, H., H. Igel, F. Gallovič, A. Cochard, and M. Ewald (2008). Source-related variations of ground motions in 3-D media: application to the Newport-Inglewood fault, Los Angeles basin, *Geophys. J. Int.*, **174,** 202–214.

Wells, D. L., and K. J. Coppersmith (1994). New empirical relationships among magnitude, rupture length, rupture width, rupture area, and surface displacement, *Bull. Seismol. Soc. Am.* **84,** 974–1002.

Wessel, P., and W. H. F. Smith (1998). New, improved version of the Generic Mapping Tools Released, *EOS Trans. AGU* **79,** 579.

Zeng, Y., J. G. Anderson, and G. Yu (1994). A composite source model for computing realistic synthetic strong ground motions, *Geophys. Res. Lett.* **21,** 725–728.

Istituto Nazionale di Geofisica e Vulcanologia
via Bassini 15
20133 Milan, Italy
ameri@mi.ingv.it
(G.A., F.P.)

Department of Geophysics
Charles University
Prague, Czech Republic
(F.G.)

Dipartimento di Scienze Fisiche
Università degli Studi
"Federico II"
Naples, Italy
(A.E.)

Manuscript received 23 February 2008